Engineering Notes

ENGINEERING NOTES are short manuscripts describing new developments or important results of a preliminary nature. These Notes cannot exceed 6 manuscript pages and 3 figures; a page of text may be substituted for a figure and vice versa. After informal review by the editors, they may be published within a few months of the date of receipt. Style requirements are the same as for regular contributions (see inside back cover).

Summary of the NASA-SRI Round Robin Ablation Program

N. K. HIESTER* AND C. F. CLARK†
Stanford Reasearch Institute, Menlo Park, Calif.
AND
N. S. VOJVODICH‡
NASA Ames Research Center, Moffett Field, Calif.

PHASE I of the NASA-SRI (Stanford Research Institute) Round Robin Ablation Program showed that a procedure for comparing ablation test results from various participating organizations, and covering both a charring (phenolic-nylon) and a noncharring (Teflon) material, is feasible.[1,2] The technique involves a dimensionless correlation of mass-loss rate $\dot{m}_t$, heating rate $\dot{q}$, and stagnation-point pressure P_{t_2}, data obtained with standard instrumentation and identical model geometry in twelve different supersonic arcjet facilities. In phase II the generality of the correlation was investigated by testing the two phase I materials plus five low-density ablators (Table 1) over wider ranges of $\dot{q}$ (50–3300 Btu/ft²-sec), stagnation enthalpy h_t (1700–34,000 Btu/lb), and P_{t_2} (0.004–30 atm). In addition, more extensive front-surface temperature, T_{FS}, and internal temperature rise, ΔT, measurements were made to see if the temperature response could be correlated in a manner similar to $\dot{m}_t$. This Note summarizes and compares the salient features and findings of this program and compares them with literature data on models of different shapes and dimensions.

Experiments

The matrix of test conditions for phase II (Fig. 1) was developed by selecting three test conditions for each participant that would utilize the full range capability of the plasma arc heater and at the same time would provide the widest distribution of test conditions for all facilities. Also shown in Fig. 1 is the envelope of conditions covered in phase I. The subsonic plasma-arc facility at the Manned Spacecraft Center, NASA Houston, also participated.

Calorimeters and flat-faced ablation models of the same shape[1] were provided by SRI to each participant who supplied test information on $\dot{q}$, P_{t_2}, h_t, T_{FS}, and ΔT. All model measurements, such as weight loss, recession, char depth, and char density, were performed at SRI. Experimental pro-

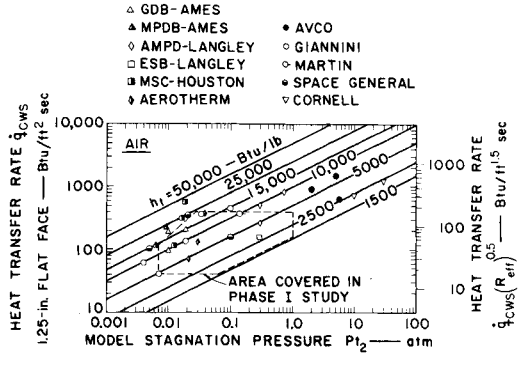

Fig. 1 Test conditions for phase II round robin.

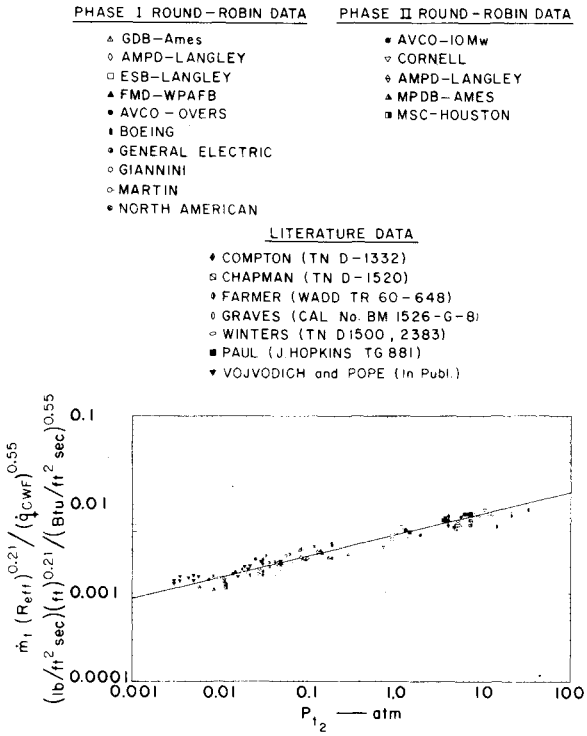

Fig. 2 Correlation of Teflon data.

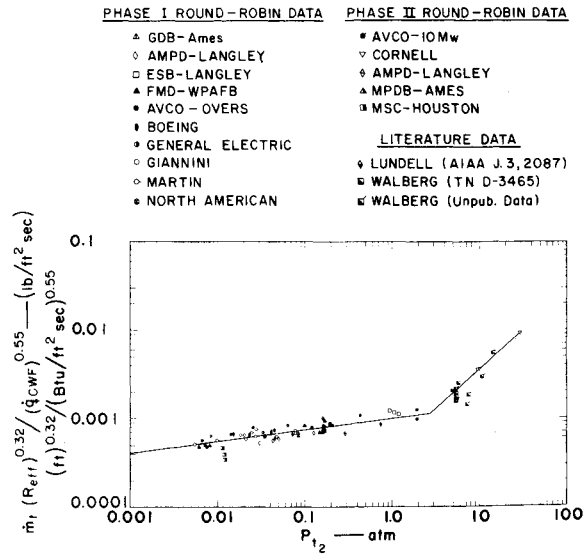

Fig. 3 Correlation of high-density phenolic-nylon data.

Received October 17, 1969; revision received April 16, 1971.

* Physical Sciences Division. Director, Materials Laboratory. Associate Fellow AIAA.
† Physical Sciencies Division. Senior Chemical Engineer.
‡ Thermo- and Gas Dynamics Division. Research Scientist. Member AIAA.

Table 1 Description of ablative materials

Code[a]	Material	Relative elemental composition	Manufacturer	Density, lb/ft³	Mode of degradation	Char yield[b]	Organic content[c]
T	Teflon	C_2F_4	duPont	135.6	Vaporization	0	...
P	Phenolic-nylon	$C_{13}H_{18}O_2N_1$	Ames	74.3	↑	0.32	0.95
PLH	Phenolic-nylon	$C_{13}H_{18}O_2N_1$	Hughes	35.7	Decomposition in depth	0.43	0.95
PLL	Phenolic-nylon	$C_{13}H_{18}O_2N_1$	Langley	35.5	to yield char residue and	0.43	0.95
A	Epoxy-novolac	$C_4H_{4.5}O_{.8}Si_{0.4}$	AVCO	31.0	percolating gases	0.55	0.50
SP	Silicone elastomer	$C_1H_3O_{.7}Si_{0.5}$	Langley	33.5	↓	0.45	0.18
SG	Silicone elastomer	$C_1H_{2.9}O_1Si_{0.6}Fe_{0.2}Al_{0.1}$	General Electric	36.8		0.90	0.10

[a] This notation, assigned by SRI in Ref. 3, is used in this discussion for material identification.
[b] Average of measurements from arcjet tests formed over a range of supersonic heating conditions.[1,3]
[c] Mass fraction of carbon in char.

cedures and results of phase II are detailed in Refs. 3 and 4. Stream calibration runs were made in each facility to measure 1) heating rates with both facility and SRI-supplied calorimeters, 2) stream enthalpies, and 3) the radial uniformity of the stream in terms of both $\dot{q}$ and P_{t_2}. These studies showed that the average stream enthalpy measured by an energy balance frequently does not represent the centerline enthalpy where the model is being tested.

Ablation behavior

The dimensional analysis approach used[4] is based on the procedures pioneered by Buckingham[5] and Rayleigh.[6] In phase I, the total mass loss data for the *high density materials* were correlated as follows:

$$\dot{m}_t = a(\dot{q}_{CWS})^n(P_{t_2})^m \tag{1}$$

The aforementioned dimensional analysis leads to

$$\dot{m}_t(R_{\text{eff}})^{1-m-n}/(\dot{q}_{CWF})^n = b(P_{t_2})^m \tag{2}$$

which is identical to Eq. (1) when the effective radius of the model R_{eff} is constant, as it was in phase I ($R_{\text{eff}} = 0.172$ ft). In these equations, a, b, m, and n are empirical constants, different for each material; $\dot{q}_{CWS}$ and $\dot{q}_{CWF}$ are the cold-wall heat fluxes measured by the Stanford calorimeter and the facility calorimeter,§ respectively.

To test the validity of the correlation, the open literature on supersonic arcjet testing was reviewed to locate additional ablation data on Teflon and high-density phenolic-nylon, with $\dot{m}_t$ and environmental parameters either tabulated or capable of being calculated. The Teflon results from phase I and the literature data (which involved varying R_{eff}) were computer-correlated by a regression program in terms of Eq. (2) which yielded $b = 0.0046$, $n = 0.55$, and $m = 0.24$. The multiple correlation coefficient K_m was 0.99, and the standard deviation σ was 11%. The closer K_m is to unity, the more meaningful is the correlation selected; the regression program adjusts b, n, and m to maximize K_m. Equation (2) with these constants for Teflon is plotted in Fig. 2, where the results of the phase II round-robin high-stagnation-pressure runs performed at AVCO and Cornell have been added; R_{eff} ranged from 0.016 to 0.55 ft. Note that the exponent m for P_{t_2} is constant, at least to 33 atm. This is reasonable, since Teflon ablates primarily by sublimation and should be little affected by mechanical forces. As a matter of interest the data obtained by Winters are from flight tests.

Table 2 Constants for Eq. (1) for phase II data[a]

Material[b]	a	n	m	K_m	σ, %
PLL	0.00465	0.36	0.26	0.96	15
PLH	0.00388	0.36	0.19	0.94	14
A	0.00357	0.47	0.33	0.97	16
SP	0.000317	0.81	0.19	0.94	24
SG	0.000188	1.03	0.28	0.92	36
T^c	0.0060	0.57	0.25	0.97	10
P^c	0.0018	0.55	0.13	0.96	10

[a] Km = multiple correlation coefficient; σ = standard deviation.
[b] See Table 1 for SRI code symbols for materials.
[c] Data from phase I round robin correlated to Eq. (1).

§ The heating rates measured with the facility calorimeters, and converted to the SRI calorimeter size and shape, were used to provide a common basis since the literature data reported only facility information.

The phenolic-nylon data from phase I gave $b = 0.0010$, $n = 0.55$, $m = 0.13$, as plotted in Fig. 3, where again the phase II high-P_{t_2} runs at Cornell and AVCO have been added. The R_{eff} span is 0.016–0.17 ft. This plot shows that at high P_{t_2} the phenolic-nylon models exhibit higher $\dot{m}_t$'s than would be predicted by the phase I correlation. However, these higher-rate data do fit a correlation line of steeper slope, with the break at $P_{t_2} \simeq 2.7$ atm. Thus, for $P_{t_2} > 2.7$ atm (and at least up to 29 atm) the relation is

$$\dot{m}_t(R_{\text{eff}})^{0.32}/(\dot{q}_{CWF})^{0.55} = 0.0048(P_{t_2})^{0.88} \tag{3}$$

This variation in behavior might have been anticipated, because phenolic-nylon, when ablating, produces an extremely fragile char which is particularly sensitive to the mechanical stresses brought on by P_{t_2}. These models showed almost no char after exposure to the high-P_{t_2} environments, and thus had reduced thermal protection. The higher exponent on the pressure term in Eq. (3) is based on this fact of char failure above a P_{t_2} of 2.7 atm, and the dimensional analysis given in Ref. 4 provides the reason for it.

The ranges of variables covered by the correlations in Figs. 2 and 3 are: $\dot{m}_t$, 95-fold for Teflon, and 85-fold for phenolic-nylon; $\dot{q}_{CW}$, 140-fold; P_{t_2}, 11,000-fold; h_{MEAS}, 36-fold; and R_{eff}, 35-fold.

For *low-density materials*, the same approach was used; since R_{eff} was constant at 0.172 ft, Eq. (1) was used for the regression analysis. For the phase II data, the values of the constants found, the degree of correlation, and the percent standard deviation are given in Table 2. The correlations are poorest for the silicone materials SP and SG, which exhibited an ablation mechanism change over the range of test environments involved; below the melting point of silica, the surface is protected by silica and some silicon carbide that is formed with the evolution of CO; above the melting point, however, SiO_2 reacts with C to form, in addition, liquid Si and gaseous SiO, which are rapidly removed from the surface.[7]

The increased standard deviation for the low-density materials is not surprising; their compositions and ablated appearance are less reproducible, and it is more difficult to measure linear dimensions on the charred cores. A plot for Avcoat Material (A) is shown in Fig. 4. The MSC-Houston

Table 3 Constants for front surface temperature, Eq. (4)

Material	a	u	v	K_m	σ, %
PLL	2870	0.107	0.052	0.94	5
PLH	2600	0.119	0.055	0.93	6
A	2280	0.127	0.025	0.90	6
SP	2110	0.129	0.028	0.93	5
SG	2680	0.0766	0.032	0.88	5

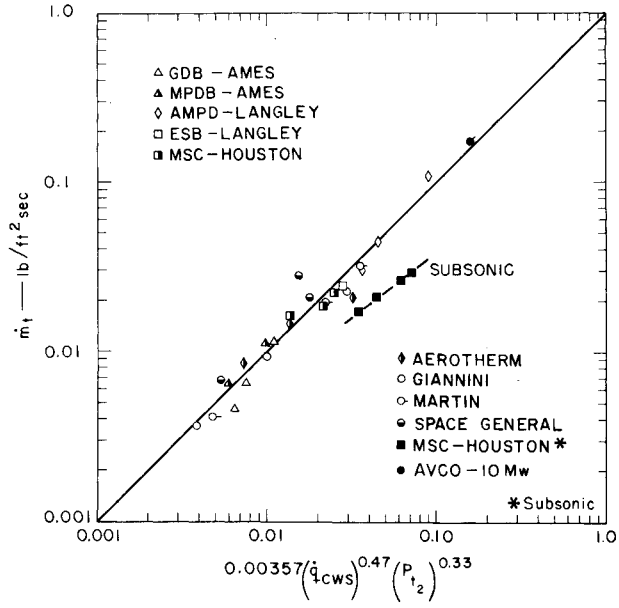

Fig. 4 Mass-loss rate correlation for Avcoat.

subsonic data, which were not used in the regression analysis, are also shown for comparison with the supersonic results.

Temperature response

The development of dimensionless forms for the temperature correlations involves additional variables, which differ for the two cases of concern: front surface and internal temperature.[3]

For front surface temperature (T_{FS},°R), the facility pyrometers were previously calibrated in place and the data from these instruments were used for correlation purposes. One of the relations evaluated was

$$T_{FS} = a(\dot{q}_{CWS})^u(P_{t_2})^v \tag{4}$$

The regression analysis gave the results shown in Table 3. Plots for two materials are given in Fig. 5. Evaluation of the T_{FS} correlations confirm that, in the lower thermal environments, the silicone materials SP and SG perform best. At a higher T_{FS} (e.g., 4500°R), their behavior is reversed, and they show the highest pyrolysis rates.

For internal temperature rise (ΔT, °F), which is of considerable interest in heat shield design, the form of the relation evaluated was

$$x = a(P_{t_2})^b(\dot{q}_{CWS})^c(t)^d(\Delta T)^e \tag{5}$$

where x is the depth in inches at which the temperature rise is measured and t the time at which it occurred. Approximately six points from the time-temperature record for each model, covering ΔT's up to ~1200°F, were used in the regression analysis. The results are given in Table 4.

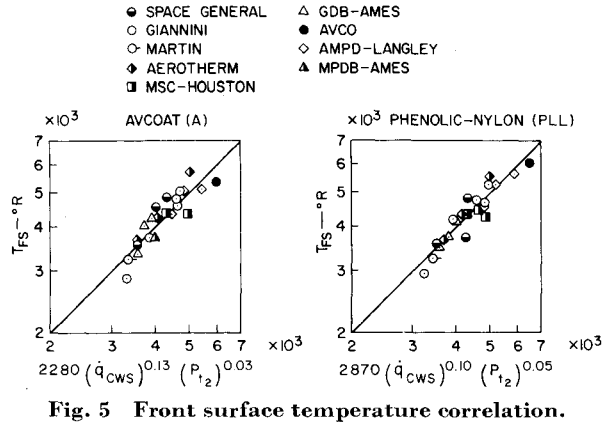

Fig. 5 Front surface temperature correlation.

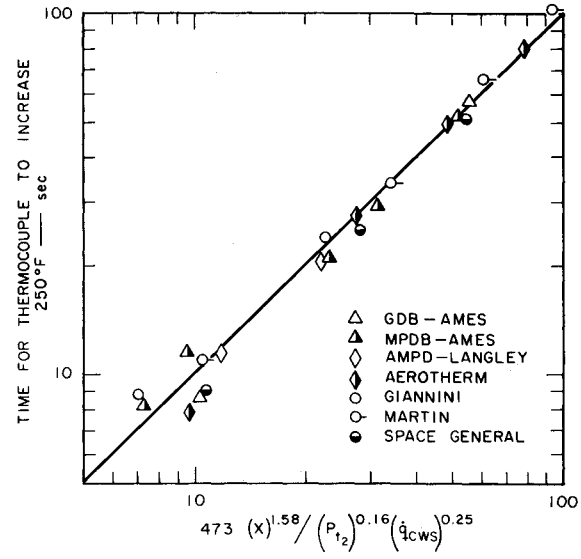

Fig. 6 Internal temperature rise correlation for Avcoat.

Chapman[2] interpreted model temperature data obtained in a subsonic facility in a similar way. For a low-density phenolic-nylon prepared at Langley (ρ = 39 lb/ft³), his relation was $x = 0.013\ \dot{q}^{0.39}t^{0.89}\Delta T^{-0.39}$. This compares to $x = 0.034\ \dot{q}^{0.30}t^{0.63}\Delta T^{-0.28}$ for (PLL) when P_{t_2} is taken as 1 atm.

Table 4 Results for internal temperature rise, Eq. (5)

Material	a	b	c	d	e	K_m	σ, %
PLL	0.034	0.053	0.30	0.63	−0.28	0.93	13
PLH	0.056	0.035	0.15	0.58	−0.24	0.97	9
A	0.037	0.018	0.27	0.60	−0.26	0.92	14
SP	0.072	0.022	0.18	0.52	−0.30	0.95	12
SG	0.12	0.031	0.098	0.54	−0.28	0.97	8

Recently, postlaunch reports[9] have become available for several of the unmanned Apollo spacecraft which used Avcoat (A) on the heat shield. Average $\dot{q}$'s and P_{t_2}'s for the re-entry exposures were used in Eq. (5) along with the appropriate constants given above to predict the positions of specific isotherms. These predictions were compared with the positions measured by NASA Manned Spacecraft Center and found to deviate no more than 25%.

A more limited correlation was evaluated in which ΔT was 250°F; for this, the time was designated t_{250}, and it was made

Table 5 Time to ΔT = 250°R, Eq. (6)

Material	a	b	c	d	K_m	σ, %
PLL	1110	−0.13	−0.33	1.54	0.98	13
PLH	930	−0.13	−0.25	1.62	0.99	8
A	470	−0.166	−0.25	1.58	0.99	9
SP	7250	+0.0074	−0.53	1.70	0.97	16
SG	370	−0.12	−0.087	1.81	0.99	5

the dependent variable

$$t_{250} = a(p_{t_2})^b(\dot{q}_{CWS})^c(x_{250})^d \tag{6}$$

Results of the regression analysis are given in Table 5 and are shown for Avcoat (A) in Fig. 6. The reduction of one variable between Eqs. (5) and (6) obviously improves K_m.

References

[1] Hiester, N. K. and Clark, C. F., "Feasibility of Standard Evaluation Procedures for Albation Materials," CR-379, 1966, NASA.

[2] Hiester, N. K. and Clark, C. F., "The Feasibility of a Standardized Ablation Test Procedure," *SAMPE Journal*, Vol. 4, No. 1, 1967, pp. 14–19.

[3] Hiester, N. K., and Clark, C. F., "Comparative Evaluation of Ablating Materials in Arc Plasma Jets," TR 111, April 1, 1965–March 31, 1968, Contract NASr-49(15), NASA CR-1207, 1968, Stanford Research Inst.

[4] Hiester, N. K., Clark, C. F., and Vojvodich, N. S., "Ablative Characterization of Seven Heat Shield Materials—A Review of the NASA-Stanford Research Institute Round-Robin Program," *AIAA/ASME 10th Structures, Structural Dynamics and Materials Conference*, AIAA, New York, 1969, pp. 57–68.

[5] Buckingham, E., "On Physically Similar Systems: Illustrations of the Use of Dimensional Analysis," *Physical Review*, Vol. 4, p. 345, 1914.

[6] Rayleigh, L., "The Principle of Similitude," *Nature*, Vol. 95, 1915, p. 66.

[7] Rosensweig, R. E. and Beecher, N., "Theory for the Ablation of Fiberglass-Reinforced Phenolic Resin," *AIAA Journal*, Vol. 1, Jan. 1963, pp. 1802–1809.

[8] Chapman, A. J., "An Experimental Investigation of Several Ablation Materials in an Electric Arc-Heated Air Jet," TND 1520, April 1963, NASA.

[9] "Postlaunch Report for Mission AS 202 (Apollo Spacecraft 009)," MSC-A-R-66-4, May 6, 1966, NASA; also "Postlaunch Report for Mission AS 202 (Apollo Spacecraft 011)," MSC-A-R-66-5, Oct. 12, 1966, NASA.

Solar Electric Missions To Ceres

DAVID R. BROOKS*
NASA Langley Research Center, Hampton, Va.

THE continuing interest shown in missions to the asteroid belt can be justified by considering the uniqueness of this region as a source of valuable information regarding the origin of the solar system and as a possible hazard for future probes enroute to the outer solar system. For studying the latter problem an asteroid belt flythrough mission is sufficient to initiate a program of accurately determining relevant properties of the region between roughly 2 and 4 a.u. However, for studying the asteroid belt itself, it appears obvious that no such effort can be considered worthwhile unless it includes at least a close flyby of one of the asteroids as a primary mission objective.

In this Note, flyby and rendezvous missions to the largest asteroid—Ceres—are examined for a late 1976 launch opportunity. The purpose of the Note is to demonstrate the application of combined chemical and solar electric propulsion (SEP) systems to a specific mission of particular scientific value and to establish approximate weight breakdowns for payload-optimized spacecraft.

The scientific return from a close approach to, or soft landing on, Ceres would be considerable, for size is the only physical property of the major asteroids which is known with reasonable certainty. A target such as Ceres, which is located in the asteroid belt, may deserve priority over easier targets such as Eros which pass closer to Earth. In this way, the information gained from what will, in any event, be a major mission effort can be maximized since an asteroid belt survey can be performed simultaneously.

Approximate orbital elements and some physical properties of Ceres are shown in Table 1. The orbital parameters are

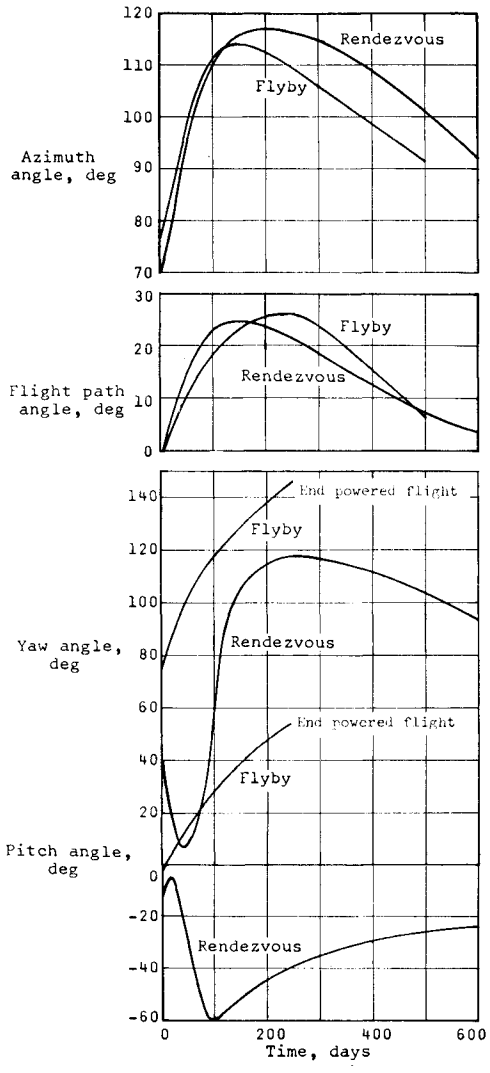

Fig. 1 Spacecraft orientation (azimuth and flight-path angles) and thrust vector orientation (yaw and pitch angles) for flyby and rendezvous missions to Ceres.

subject to large (compared to the major planets) periodic fluctuations due primarily to Jupiter, so it is desirable to use osculating (time variable) elements even for preliminary studies. For this purpose, an ephemeris tape was generated from data computed by Michielsen and Krop[1] similar to the tabular data for Ceres and Vesta found in the NASA Planetary Flight Handbook.[2]

Table 1 Orbital and physical characteristics of Ceres

Inclination to ecliptic (deg)	10.607
Longitude of ascending node (deg)	80.514
Longitude of perihelion (deg)	152.367
Mean motion (deg/day)	0.2141
Mean circular velocity (EMOS)	0.6011
Eccentricity	0.0759
Sidereal period (yr)	4.60
Semimajor axis (a.u.)	2.7675
Perihelion (a.u.)	2.5574
Aphelion (a.u.)	2.9776
Mean anomaly at epoch (deg)[a]	279.880
Diameter (statute miles)	480.0
Mass (fraction of Earth)[b]	2.2×10^{-4}
Escape velocity (m/sec)[c]	680.0
Albedo	0.06
Rotational period (hr)	9.08

[a] Epoch June 11, 1957.
[b] Assuming asteroid density equal to Earth's density. Based on Lunar density, the mass would be multiplied by approximately 0.6.
[c] Based on mass as given.

Presented as part of Paper 70-1120 at the AIAA 8th Electric Propulsion Conference, Stanford, Calif., August 31–September 2, 1970; submitted October 19, 1970; revision received April 19, 1971.

* Aerospace Engineer, Mission Analysis Section, Mission Analysis and Applications Branch, Space Technology Division. Member AIAA.